

Positioning of quantum dots on metallic nanostructures

R K Kramer^{1,2}, N Pholchai¹, V J Sorger¹, T J Yim¹, R Oulton¹ and X Zhang¹

¹ NSF Nanoscale Science and Engineering Center, University of California, Berkeley, CA, USA

² School of Engineering and Applied Sciences, Harvard University, Cambridge, MA, USA

E-mail: xiang@berkeley.edu

Received 29 September 2009, in final form 8 December 2009

Published 16 March 2010

Online at stacks.iop.org/Nano/21/145307

Abstract

The capability to position individual emitters, such as quantum dots, near metallic nanostructures is highly desirable for constructing active optical devices that can manipulate light at the single photon level. The emergence of the field of plasmonics as a means to confine light now introduces a need for high precision and reliability in positioning any source of emission, which has thus far been elusive. Placing an emission source within the influence of plasmonic structures now requires accuracy approaching molecular length scales. In this paper we report the ability to reliably position nanoscale functional objects, specifically quantum dots, with sub-100-nm accuracy, which is several times smaller than the diffraction limit of a quantum dot's emission light. Electron beam lithography-defined masks on metallic surfaces and a series of surface chemical functionalization processes allow the programmed assembly of DNA-linked colloidal quantum dots. The quantum dots are successfully functionalized to areas as small as $(100 \text{ nm})^2$ using the specific binding of thiolated DNA to Au/Ag, and exploiting the streptavidin–biotin interaction. An analysis of the reproducibility of the process for various pattern sizes shows that this technique is potentially scalable to the single quantum dot level with 50 nm accuracy accompanied by a moderate reduction in yield.

(Some figures in this article are in colour only in the electronic version)

1. Introduction

In order to exploit the quantum nature of light, it is important to realize optical systems that can isolate the interaction of a single electronic transition of a single mode of light. The emerging field of nano-optics [1] now points to new ways to strengthen this interaction between light and matter by using metallic nanostructures to confine light well below its wavelength [2, 3]. However, placing an emission source in the vicinity of such tightly bound optical modes requires positioning accuracy on molecular length scales, which is currently a key problem in nano-optics [4]. While positioning accuracy remains a challenge, the specific placement of single quantum dots (QDs) remains a distant goal. In this paper we report on the ability to successfully position a small number of QDs on a metallic surface with 100 nm accuracy and discuss the potential of this method to functionalize individual dots to 50 nm. The use of chemical functionalization and specific binding is appealing in this case as it has the

potential to achieve the necessary molecular length scale accuracy and, with it, the prospect of positioning single QDs. Relevant applications for this technique include integration of nano-emitters in optical cavities [5–7], nanowires [3, 8] and waveguides [9, 10].

Existing methods for positioning nano-particles are elusive given the aforementioned constraints on accuracy. Bimberg *et al* [11] reported the fabrication of nanoscale QDs with good optical properties using a natural-growth mode of strained-layer semiconductors. The Stranski–Krastanow growth method produces InAs [12] or CdSe [13] QDs at telecom and visible wavelengths, respectively. One considerable disadvantage to this technique is the inability to control where QDs form and their size due to the spontaneous nature of the growth. This problem has been partially solved by growing the QDs on a surface patterned with nano-sized holes, which define a strain field in which the QDs form [14–17]. However, this method is only partially compatible with the growth conditions of the surrounding optical structures.

Cui *et al* [18] have reported the use of capillary forces to assemble nano-particles. However, liquid-phase deposition of nanocrystals into grooves using capillary forces requires specific control of the evaporation rate, liquid–substrate surface tension and many other parameters which are difficult to characterize and reproduce. These approaches all utilize some form of nanoscale patterning along with a force related to the pattern's configuration. Alternative approaches are emerging that functionalize the pattern itself, for example with a self-assembled monolayer of molecules which are designed to specifically bind to the functional object. Wang *et al* [9] have reported on a QD waveguide device for which fabrication was demonstrated through DNA-mediated self-assembly on Si/SiO₂ and the smallest functionalized length was 1 μm . DNA-based hybrid nano-assembly has also been used for nano-particles [19–22], carbon nanotubes [23] and multimetal microrods [24]. Protein-based methods [25, 26] have also been reported to show functionalization to metallic surfaces, but require the underlying substrate to be non-metallic since removal of the photoresist cannot be accommodated. Also, almost all previously reported methods are based on bottom-up approaches, which intrinsically have higher defects and are harder to control.

Here, we report the ability to successfully position a small number of colloidal QDs to within less than 100 nm accuracy on metallic surfaces via combined top-down fabrication and bottom-up assembly. In this work, a DNA-mediated process for programmed assembly of QDs [9, 10, 27, 28] has been adapted to accommodate gold or silver surfaces, i.e. for plasmonic structures. Electron beam lithography (EBL) was used to create chemical binding sites via predetermined openings in the photoresist film, thus exposing the underlying metal surface at predetermined locations. In subsequent assembly steps (further) chemical reactions will be restricted to these binding sites.

The QD functionalization is carried out with a double chemical *key–lock* system. The key feature hereby is single-stranded DNA (ssDNA) providing both the anchor to the substrate and selective binding to the QD. While a thiol group on one end of the ssDNA enables selective binding to the hydrophilic substrate, a biotin group at the other end provides a docking mechanism for the QD. The QDs used in this study are covered with a streptavidin layer that has been proven to selectively bind to the biotin from the ssDNA [9]. The stock 1 μM aqueous solution of streptavidin-conjugated CdSe/ZnS core–shell QDs (Q10021MP) were obtained from Invitrogen. Each streptavidin molecule (a four-unit protein) having a size of 5 nm adds to the original dimension of CdSe/ZnS QDs (~ 5 nm). This method provides for desired QD positioning on metallic surfaces, which is a critical step in nanoscale optics.

2. Fabrication

Substrates were prepared by evaporation of gold or silver onto a thin adhesion layer (Cr) on a Si-wafer with a user-defined PMMA pattern written by EBL. The wafers were cleaved and subsequently washed with xylene, acetone, isopropyl alcohol (IPA) and de-ionized (DI) water and blown dry with

a N₂ gun. A 3% dilution of PMMA (A3) was spin-coated, yielding an approximately 90 nm thick layer (4000 rpm for 48 s), followed by a solvent dry-out step (180 °C for 20 min). Standard EBL was carried out to define the binding sites. After exposure, samples were developed in 1:3 (v:v) methyl isobutyl ketone (MIBK):IPA (70 s), rinsed with IPA and blown dry with a N₂ gun. It was important to create a hydrophilic metal substrate to ensure proper binding of the electronegatively charged thiol group of the ssDNA. A mild Ar-plasma etch (20 W for 10 s) provides a viable compromise between the desired surface preparation and parasitic photoresist etching. Immediately after the plasma treatment the DNA solution (diluted to 50 μM with PBS) was drop-casted onto the samples. For the following resting step (24 h), samples were placed in a home-made humidified chamber to ensure proper interaction between the DNA and the substrate. The DNA (Integrated DNA Technologies) used in this work was defined by linker modifications 5' biotin–TEG (triethylene glycol) and 3' thiol modifier C3 S–S (disulfide). For the first surface chemical reaction, the DNA thiol modifier C3 S–S (disulfide) allows the DNA to bind to the gold surface. The gold–sulfide bond is strong and provides the functionality of the self-assembled monolayer (SAM).

After the resting step, samples were rinsed with 1 \times PBS to wash off unbound DNA. Due to the lack of rigidity of ssDNA, the surface-bound DNA molecules can have many different conformations or entanglements with neighboring molecules [29], which may suppress the biotin linkers' affinity to bind with streptavidin-conjugated QDs. Therefore, samples were submerged in 6-mercapto-1-hexanol (MCH) (2 μl) and PBS (3 ml) solution (1 min) to enable passivation of the DNA self-assembly. MCH contains a sulfhydryl (thiol) group and hydroxyl (alcohol) group at each end of a 6-carbon, or 11.8 Å [30], spacer arm, which forces the ssDNA upright to perform as a hook for the next chemical reaction. Prior to the QD functionalization step, samples were post-rinsed with PBS to remove any excess and unbound DNA and/or MCH molecules. Streptavidin-coated QDs were drop-casted on the surface and samples were placed back in the humidified chamber ($t > 30$ min). Immersing the entire sample in PBS (5 min) was found to remove any excess QDs and/or other unbound particles. Finally, the PMMA photoresist layer was lifted-off with dichloromethane (3 min) followed by drying the samples in ambient air. Figure 1(a) summarizes the individual steps for the functionalization process. Testing the protocol on a flat substrate, we found clear signatures of successfully functionalized QDs from an atomic force microscope (AFM) image (figure 1(b)). The measured height (z -direction) of single *bumps* was found to be about 17 nm, corresponding well to the QD dimension of 15 nm. In addition, a surface scan of a control sample consisting of a gold (Au) film atop a silicon (Si) substrate shows a very low surface roughness (< 1 nm rms) without the signature of any bump-like features.

3. Results

In order to test the size dependency of the programmability, binding sites, referred to hereafter as *patterns*, of various sizes

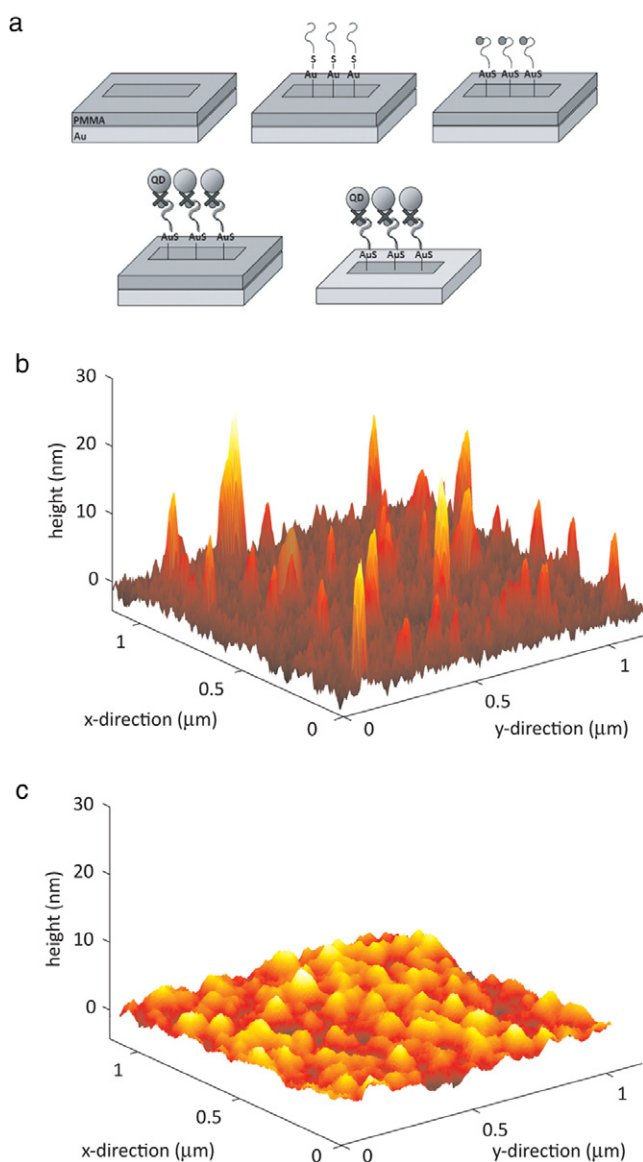


Figure 1. Two layer assembly of QD patterns. (a) EBL pattern the PMMA-coated metallic substrate, treat with plasma etch; deposit thiol and biotinylated DNA, deposit 6-mercapto-1-hexanol (MCH) to act as a spacer and expose biotin groups at the surface; deposit streptavidin-coated QDs; remove PMMA by immersion in dichloromethane. (b) AFM image of sparsely functionalized QDs on a gold substrate. The surfaces roughness is characterized as approximately 1 nm, and single QDs are ~ 17 nm in diameter. (c) Control AFM scan of a gold film.

were fabricated and the assembly process tested. Successful QD functionalization, ranging from large scale ($4 \times 4 \mu\text{m}^2$) down to small scale ($0.1 \times 0.1 \mu\text{m}^2$) binding sites, demonstrates the scalability and control of the process down to only a few QDs (inset figure 2(a)). High resolution scanning electron microscopy (SEM) images reveal individual QD resolution of the intended binding sites and allow for an analysis of QD density and quality of the functionalization process (figure 2(a)). We verified the optical quality of functionalized QDs by exciting them optically below the band gap energy. Indeed we found the characteristic red

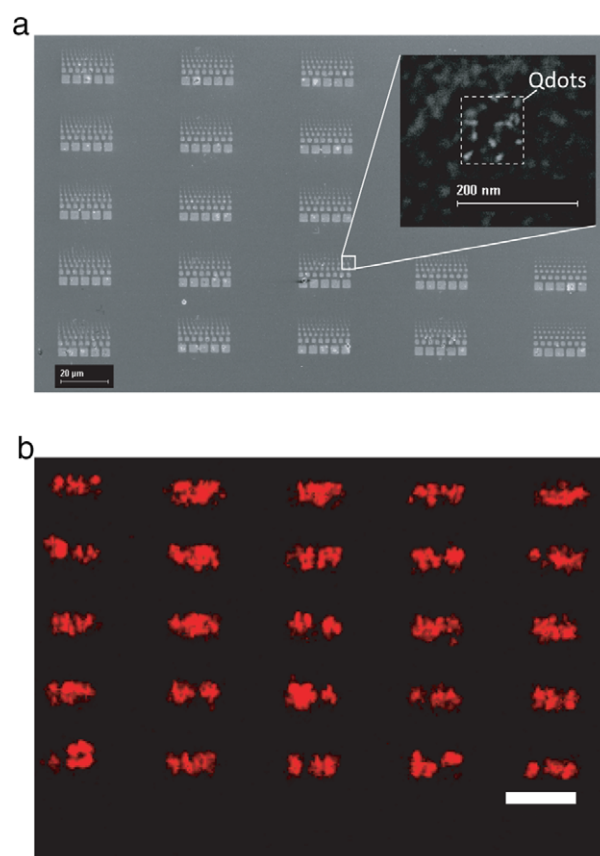


Figure 2. Functionalization of DNA-directed self-assembled QDs. (a) Scanning electron microscope image of a 5×5 array of successfully patterned QDs of variously sized square binding sites. Pattern feature lengths are $4 \mu\text{m}$, $2 \mu\text{m}$, $1 \mu\text{m}$, 500 nm , 250 nm and 100 nm . Inset: a patterned 100 nm square area of functionalized QDs (dashed line indicates the intended binding site). (b) Functionalized CdSe QDs show photoluminescence under optical excitation ($\lambda_{\text{pump}} = 488 \text{ nm}$) below the band edge as red glowing areas in a confocal microscope image. Scale bar: $30 \mu\text{m}$.

emission of CdSe quantum dots as a bright signal in contrast to unfunctionalized areas (figure 2(b)). Detailed pattern features in this fluorescence image are poorly resolved due to limited spatial resolution and detection sensitivity of our imaging system and not protocol limitations. That is, an SEM scan arguably shows sharp functionalized QD features down to the deep sub-micrometer level (figure 2(a)).

Figure 3(a) verifies a square law behavior for the average number of QDs functionalized in the various square sized patterns. The QD numbers and the error bars scale with the square of the feature length and $1/\sqrt{n}$, respectively, where n is the average number of QDs per pattern size. We have used a Matlab[®] image segmentation program to locate and count the number of QDs within squares. For a square with an area greater than $(0.5 \mu\text{m})^2$, individual QDs could not be resolved while viewing the entire square. However, partial images of the square up to QD resolution were obtained to gain information about the QD packing density. The algorithm was developed to count QDs in randomly selected 100 nm square areas of a partial image providing an average density output, which was subsequently multiplied by the total functionalized area of

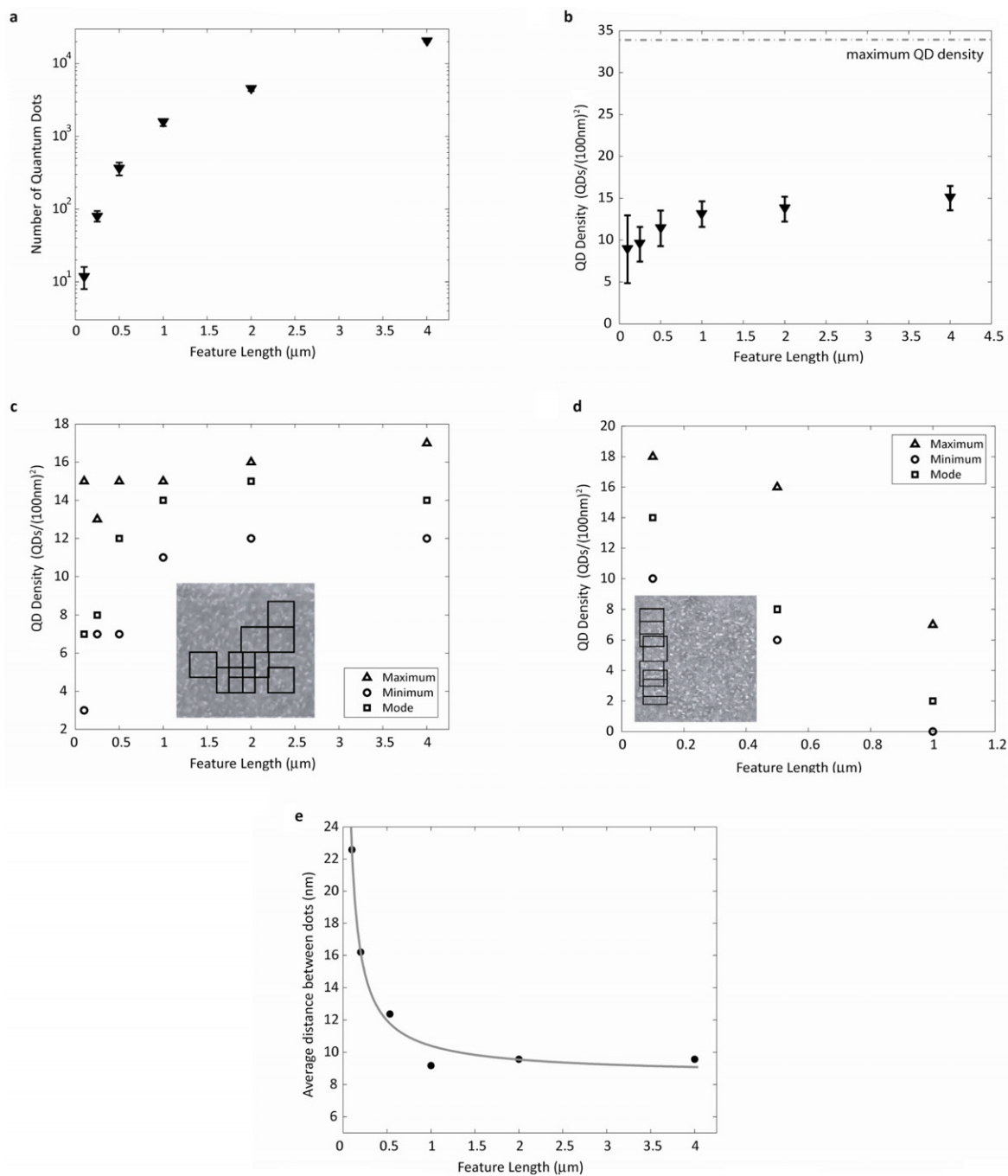


Figure 3. A (Matlab) algorithm was implemented to analyze scanning electron microscope images of functionalized QDs in differently sized binding sites. (a) The total number of QDs for various pattern sizes, which shows quadratic polynomial behavior. (b) Average QD density of various pattern sizes from arbitrarily selected $(100\text{ nm})^2$ areas within each pattern size. The maximum possible QD density was $34\text{ QDs}/(100\text{ nm})^2$. Average QD density was calculated from a set of ten arbitrarily (random) selected 100 nm square areas within each pattern size. The error bars represent the span of the collected data. (c) Maximum, minimum and modal (most commonly repeated) QD densities versus feature length from random $(100\text{ nm})^2$ areas within the central regions of patterns. Inset, $(500\text{ nm})^2$ pattern. (d) QD density versus pattern length near the edges of the smaller patterns as defined by the outermost dot. Inset, $(500\text{ nm})^2$ pattern. The QD density increased with reduction of pattern length. Towards the edges, QDs tended to clump together, making the distances between them very small, but QD density was still low. In the innermost region, QDs were more uniformly distributed. (e) Average distance between QDs per pattern sizes.

the square. The total functionalized area was estimated from an image of the entire square and characterized by grayscale numerical pixel value (image segmentation). The algorithm output an approximation of the total number of functionalized QDs in the square.

For an analysis of the QD density, arbitrarily selected 100 nm square areas within each pattern size were selected (figures 3(b)–(d)). While the average QD density increased with increasing pattern size in squares with a feature length less than $1\ \mu\text{m}$, larger squares show nearly constant average

QD densities. Similarly, QD density fluctuations were largest for the smallest patterns and remained nearly constant across larger pattern sizes. This indicates that for squares with a feature length greater than 1 μm , the QD packing density is determined by the surface functionalization of Au–thiol–DNA rather than pattern area. This is consistent with results for the maximum packing density of the smaller patterns, which was found to be nearly equal to the maximum packing density of larger patterns (figure 3(c)). Since the streptavidin-coated QDs are approximately 17 nm in diameter (measured by AFM), the maximum *possible* packing QD density could be 34 QDs/(100 nm)². This yields a maximum packing density of approximately 50% for all pattern sizes.

With a reduction of pattern size, the photoresist thickness and edge effects of the EBL process become increasingly important for the QD packing density. The reduction of the mode and minimum QD density value for small patterns shows statistical limitations potentially brought on by these edge (fringing) effects (figure 3(c)). To further investigate this, an algorithm was executed to analyze the relative configuration of dots in different regions of the smaller ($A_{\text{pattern}} < 4 \mu\text{m}^2$) QD-functionalized patterns (figure 3(d)). The algorithm determined the number of dots and distances between nearest-neighboring dots in ten arbitrarily selected 100 nm square areas with close proximity to both the center and edges of the patterns (figures 3(c) and (d)). As shown by figure 3(d), functionalization in the smallest squares was more uniform than functionalization close the edge of slightly larger squares. Near the edges, QDs tended to clump together, yielding small distances between dots, yet the density of dots was still relatively low. Near the middle of the patterns, QDs were more uniformly distributed and distances between dots were more consistent. Figure 3(e) shows the average distance between QDs for entire patterns.

Notice that functionalization appears to have improved slightly with reduction in pattern size. Specifically, figure 3(d) shows that functionalization of QDs in 100 nm squares was slightly better than functionalization close the edges of other larger squares. An explanation of this phenomenon is not definite, yet we hypothesize that in larger squares, the edges of the pattern never come into contact with the drop-casted solutions due to surface tension of the liquid. Smaller squares (with an increased aspect ratio) may have the added benefit of a capillary action to draw solution in towards the substrate. Alternatively, reducing the pattern area, the size of a square may simply define a radius of curvature for an inset liquid droplet, causing the actual functionalized area to be circular rather than square, which is consistent with the images in figure 2. While this eliminates binding in the corners of the patterns, it provides for good binding at the center.

The functionalization process reported here strives for a monolayer of uniform and well dispersed QDs, yet QD density appears to be limited by constraints of the surface chemical process (more so than pattern size). Firstly, the DNA packing density was limited by the effectiveness of the thiol binding to the Au surface with enhanced hydrophilicity of the surface by the plasma treatment. Once bound, the DNA may not diffuse and organize a monolayer on the Au surface due

to entanglement and spatial configuration. While the MCH spacers force the DNA into an upright position, they also space the DNA apart and suppress the closest packing density. The effectiveness of the MCH spacers was not quantified in this report, leaving the possibility of unexposed biotin groups. Moreover, any variation in the uniformity of charge of the immobilized DNA would ultimately yield non-uniform QD binding. Lastly, multiple rinsing steps introduce loss of binding throughout.

4. Conclusion

In summary, control over small numbers (~ 10) of nanoscale functional objects (QDs) to within less than 100 nm accuracy has been demonstrated. We have introduced a self-assembly fabrication method for positioning colloidal QDs on metallic substrates. Highly discriminatory binding sites for QDs were defined by electron beam lithography and a DNA-mediated process. Testing QD functionalization in variously sized binding sites yielded a maximum packing density of 50% for all pattern sizes. Edge effects and statistical limitations became more apparent with reduction of pattern size, yet the highest achievable packing density was consistent for all pattern sizes. This suggests that the chemical functionalization limited the packing density of QDs more than the pattern size, and denotes the potential for fabricating single QDs in small patterns with high accuracy. With this demonstrated potential to increase control over the positioning of a small number of functionalized nano-particles, we can envision nano-optical devices that utilize QDs as optical emitters, thus allowing the frontier of optics research to access molecular length scales.

Acknowledgments

The authors thank the National Science Foundation (NSF) NSEC (DMI-0327077). R Kramer thanks the NSF Graduate Fellowship Program for financial support. Work was performed in part at the University of California, Berkeley Microfabrication Laboratory and we hereby acknowledge the Welch Foundation.

References

- [1] Novotny L and Hecht B 2006 *Principles of Nano-Optics* (New York: Cambridge University Press)
- [2] Anger P, Bharadwaj P and Novotny L 2006 Enhancement and quenching of single-molecule fluorescence *Phys. Rev. Lett.* **96** 113002–4
- [3] Akimov A V, Mukherjee A, Yu C L, Chang D E, Zibrov A S, Hemmer P R, Park H and Lukin M D 2007 Generation of single optical plasmons in metallic nanowires coupled to quantum dots *Nature* **450** 402–6
- [4] Shields A J 2007 Semiconductor quantum light sources *Nat. Photon.* **1** 215–23
- [5] Vahala K J 2003 Optical microcavities *Nature* **424** 839–46
- [6] Barnes W L, Björk G, Gérard J M, Jonsson P, Wasey J A E, Worthing P T and Zwiller V 2002 Solid-state single-photon sources: light collection strategies *Eur. Phys. J. D* **18** 197–210

- [7] Reithmaier J P, Sek G, Löffler A, Hofmann C, Kuhn S, Reitzenstein S, Keldysh L V, Kulakovskii V D, Reinecke T L and Forchel A 2004 Strong coupling in a single quantum dot-semiconductor microcavity system *Nature* **432** 197–200
- [8] Yan H, Park S H, Finkelstein G, Reif J and LaBean T H 2003 DNA-templated self-assembly of protein arrays and highly conductive nanowires *Science* **301** 1882–4
- [9] Wang C J, Huang L, Parviz B A and Lin L Y 2006 Subdiffraction photon guidance by quantum-dot cascades *Nano Lett.* **6** 2549–53
- [10] Wang C J, Parviz B A and Lin L Y 2008 Two-dimensional array self-assembled quantum dot sub-diffraction waveguides with low loss and low crosstalk *Nanotechnology* **19** 295201
- [11] Bimberg D, Grundmann M and Ledentsov N N 1999 *Quantum Dot Heterostructures* (Chichester: Wiley)
- [12] Ramachandran T R, Madhukar A, Mukhametzhanov I, Heitz R, Kalburge A, Xie Q and Chen P 1998 Nature of Stranski–Krastanow growth of InAs on GaAs(001) *J. Vac. Sci. Technol.* **16** 1330–3
- [13] Schikora D, Schwedhelm S, As D J, Lischka K, Litvinov D, Rosenauer A, Gerthsen D, Strassburg M, Hoffmann A and Bimberg D 2000 Investigations on the Stranski–Krastanow growth of CdSe quantum dots *Appl. Phys. Lett.* **76** 418
- [14] Song H Z, Usuki T, Hirose S, Takemoto K, Nakata Y and Yokoyama N 2005 Site-controlled photoluminescence at telecommunication wavelength from InAs/InP quantum dots *Appl. Phys. Lett.* **86** 113118
- [15] Atkinson P, Ward M B, Bremner S P, Anderson D, Farrow T, Jones G A C, Shields A J and Ritchie D A 2006 Site control of InAs quantum dots using *ex situ* electron-beam lithographic patterning of GaAs substrates *Japan. J. Appl. Phys.* **45** 2519–21
- [16] Sunner T, Schneider C, Straub M, Huggenberger A, Wiener D, Hofling S, Kamp M and Forchel A 2008 Scalable fabrication of optical resonators with embedded, site-controlled quantum dots *Opt. Lett.* **33** 1759
- [17] Ishikawa T, Nishimura T, Kohmoto S and Asakawa K 2000 Site-controlled InAs single quantum-dot structures on GaAs surfaces patterned by *in situ* electron-beam lithography *Appl. Phys. Lett.* **76** 167
- [18] Cui Y, Björk M T, Liddle J A, Sönnichsen C, Boussert B and Alivisatos A P 2004 Integration of colloidal nanocrystals into lithographically patterned devices *Nano Lett.* **4** 1093–8
- [19] Sastry M, Ashavani K, Datar S, Dharmadhikari C V and Ganesh K N 2001 DNA-mediated electrostatic assembly of gold nanoparticles into linear arrays by a simple drop-coating procedure *Appl. Phys. Lett.* **78** 2943
- [20] Dulkeith E, Ringler M, Klar T A, Feldmann J, Munoz Javier A and Parak W J 2005 Gold nanoparticles quench fluorescence by phase induced radiative rate suppression *Nano Lett.* **5** 585
- [21] Lakowicz J R 2006 Plasmonics in biology and plasmon-controlled fluorescence *Plasmonics* **1** 5
- [22] Chen Y, Munechika K and Ginger D S 2007 Dependence of fluorescence intensity on the spectral overlap between fluorophores and plasmon resonant single silver nanoparticles *Nano Lett.* **7** 690
- [23] Hazani M, Hennrich F, Kappes M, Naaman R, Peled D, Sidorov V and Shvarts D 2004 DNA-mediated self-assembly of carbon nanotube-based electronic devices *Chem. Phys. Lett.* **391** 389–92
- [24] Nicewarner-Pena S R, Freeman R G, Reiss B D, He L, Pena D J, Walton I D, Cromer R, Keating C D and Natan M J 2001 Submicrometer metallic barcodes *Science* **294** 137
- [25] Malicka J, Gryczynski I, Gryczynski Z and Lakowicz J R 2003 Effects of fluorophore-to-silver distance on the emission of cyanine-dye-labeled oligonucleotides *Anal. Biochem.* **315** 57
- [26] Zin M T, Leong K, Wong N Y, Hong M, Sarikaya M and Jen A K Y 2009 *Nanotechnology* **20** 015305
- [27] Storhoff J J and Mirkin C A 1999 Programmed materials synthesis with DNA *Chem. Rev.* **99** 1849–62
- [28] Hu W, Sarveswaran K, Lieberman M and Bernstein G H 2005 High-resolution electron beam lithography and DNA nano-patterning for molecular QCA *IEEE Trans. Nanotechnol.* **4** 312–6
- [29] Murphy M C, Rasnik I, Cheng W, Lohman T M and Ha T 2004 Probing single-stranded DNA conformational flexibility using fluorescence spectroscopy *Biophys. J.* **86** 2530–7
- [30] Tan H, Zhan T and Fan W Y 2006 Direct functionalization of the hydroxyl group of the 6-mercapto-1-hexanol (MCH) ligand attached to gold nanoclusters *J. Phys. Chem. B* **110** 21690–3